Visualisation of Thermal Contact with a Commercial CCD Video System

H D Falter, D Ciric, F D Long.

JET Joint Undertaking, Abingdon, Oxon, OX14 3EA, UK.

Summary

The integrity of the thermal contact between armour material and actively cooled heat sink can be visualised by cooling the component below the freezing point of water. If the component is cold enough the surface will quickly be covered by frost from the humidity in the air. Running water through the cooling channels will heat the component and the surface will defrost. Regions with reduced thermal contact can be identified by a delayed defrosting. Comparisons with tests done with a infrared thermal imaging system and with power test in the JET Neutral Beam Test Bed prove that the test gives viable results.

1 INTRODUCTION

Actively cooled dump plates in Fusion devices are made of composite materials with beryllium or Carbon Fibre Composites (CFC) as armour materials and copper alloys or molybdenum alloys as heat sinks. The heat flux can be as high as 15 - 20 MW/m^2 and requires a perfect joint between heat sink and armour. Testing of these joints is normally performed by heating the armour tile in vacuum with an electron - or ion beam. Power densities of several MW/m^2 are required for a good assessment of the braze joints[1,2]. Ultrasonic examinations and X-ray applications have been used with some success to monitor the integrity of the braze [1].

The easiest way to produce thermal gradients is probably to flow water through the cooling channel of a preheated or precooled test section. Faults in the thermal contact between heat sink and armour will show up as a distortion of the temperature distribution on the surface. All that is required is a sufficiently fast and accurate measurement of the surface temperature distribution.

As every driver knows from the heated rear windscreen of this car, defrosting starts above the heating wire and then the defrosted zone spreads away from the wire. The transition between frosted and defrosted zone is sharp, well defined, and clearly visible. Using this observation we can visualise the heat transfer from the heat sink to the armour by monitoring the defrosting sequence. We demonstrate in this paper, that the frequency and resolution of commercial domestic TV equipment is sufficient to visualise significant faults in thermal contact between armour and heat sink of divertor test sections.

2 EXPERIMENTAL SET-UP.

To start with the test section is cooled down in a conventional chest freezer to approximately -15 to -20 °C. When the cold test section is exposed to air the surface gradually covers with frost. This frost coverage will be denser if the humidity in the air is increased (hot water near by). The frosted, cold component is then heated up by flowing tap water through the water channels. The defrosting is filmed with a commercial CCD camera from a distance of approximately 1 metre. The process is recorded with

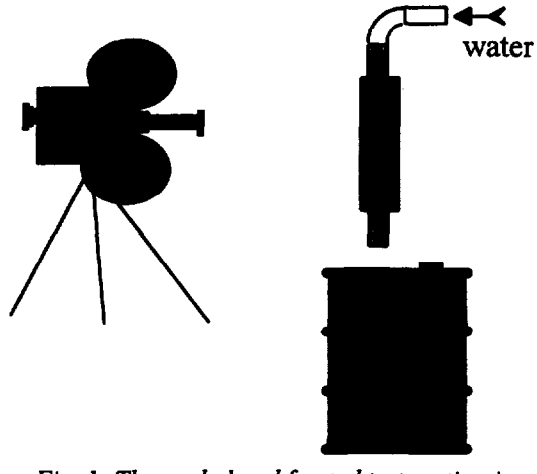

Fig. 1: The cooled and frosted test section is heated up with tap water and the defrosting is monitored.

a S VHS [4] video recorder. With a mirror behind the test section, all 4 sides of the test section can be monitored simultaneously.

The examination of the test section is carried out using a slow motion replay in which the spreading of the defrosting is observed. Areas with reduced thermal contact will show a delayed defrosting.

3 RESULTS

3.1 CFC divertor test sections

We have applied the frosting test to a number of different test sections, mainly Carbon Fibre Composites (CFC) blocks brazed onto a cooling pipe through the centre of the CFC tile.

A typical defrosting sequence is shown in Fig. 2 for a test section with 17 CFC tiles of 27 x 19 x 6 mm^3 brazed to a TZM pipe of 12.7 mm external diameter. Water flow direction during the defrosting is from right to left.

The top picture of the defrosting sequence shows that the two end tile defrost first. The second and third picture from the top show frost on exactly those tiles which had an increased surface temperature during beam exposure (tiles 3 and 11) as shown by the surface temperature profile above the defrosting sequence. This temperature distribution was measured with an IR imaging system after exposure to an energetic particle beam. The vertical grid lines in the profile correspond approximately to the gaps between the tiles. The exposed surface during beam testing was the forward facing surface in Fig. 2. We also note that the defrosting of one tile is not uniform in the sense that the surface of one side can defrost before or after the neighbouring surface of the same tile.

In the case of Fig. 2 the test section was cooled to -200 °C and the tiles have to be warmed up by approximately 200 °C before defrosting occurs. This warm-up time is long compared with the time the water needs to flow through the test section and we can detect all faults in one frame - the frame in the middle of the defrosting sequence in Fig. 2.

If we use a conventional freezer to cool the component, the temperature is much higher (-15°C) and the heat-up time is much shorter, so that the water velocity can not be neglected. This is demonstrated in Fig. 3: Again water flows from right to left and defrosting is expected to proceed from right to

Fig. 2: Defrosting sequence of a CFC monoblock test section with the surface temperature distribution during beam exposure (top) and the defrosting sequence below.

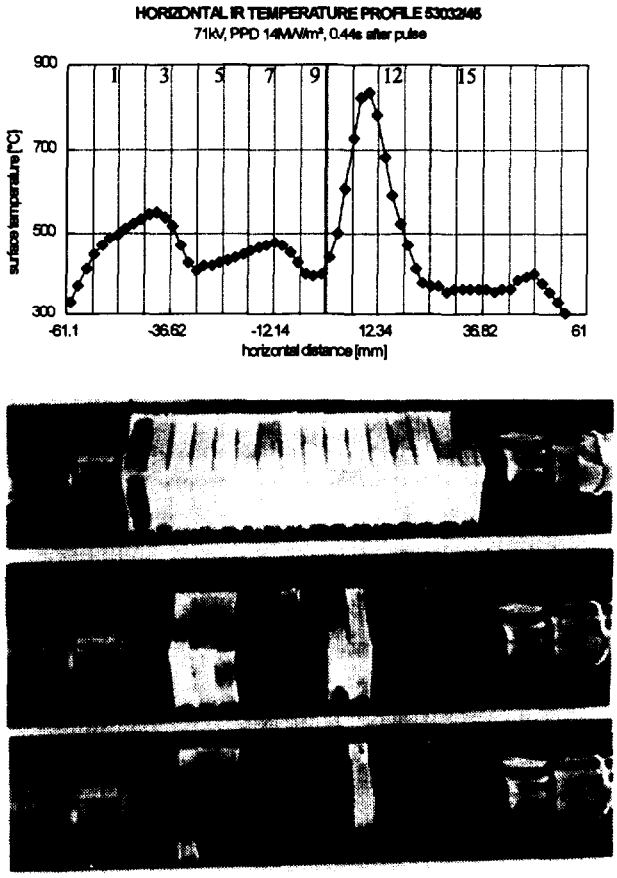

left. The first picture of the defrosting sequence indicates (just) that the second tile from the right defrosts before the first tile from right and hence that the first tile from the right has a bad thermal contact. The second picture of the defrosting sequence (some hundred milliseconds later) shows the first three tiles at the right fully defrosted. Of the next three tiles the one in the middle (tile 6) is clearly delayed with respect to its neighbours (tiles 5 & 7) and we conclude that tile 6 also has a reduced thermal contact.

Finally on the last picture of the defrosting sequence we see that tiles 3 and 4 are clearly delayed.

Fig. 5: Defrosting of an accelerator grid with some blocked water channels

The test is carried out as with the divertor test sections: The grid is cooled down in a freezer, frosted over and heated to room temperature with tap water flowing through the grids.

The result of the defrosting test is shown in Fig. 5. The first five channels from left to right are blocked by the internal frozen water in the channel, the next cooling channel (channel 6) is free, channel 7 is blocked, and all the channels right from channel 7 are free. The same defrosting sequence was also monitored with an infrared imaging system and the result is shown in Fig. 6. The grey scale in Fig. 6 matches that of Fig. 5 with black for warm (unfrosted) and white for cold (frosted). Again we can identify blocked channels but the resolution from defrosting appears to be better. In fact using the complete defrosting sequence the detailed structure of the cooling channels can be visualised. Fig. 7 shows a frame in which the water is supplied from the left. We can see the water manifold at the left and the individual channels leading into the grid area. We can also see the individual channels exiting from the grid at the right.

Fig. 6: Warm-up sequence of Fig. 5 recorded with a thermal imaging system.

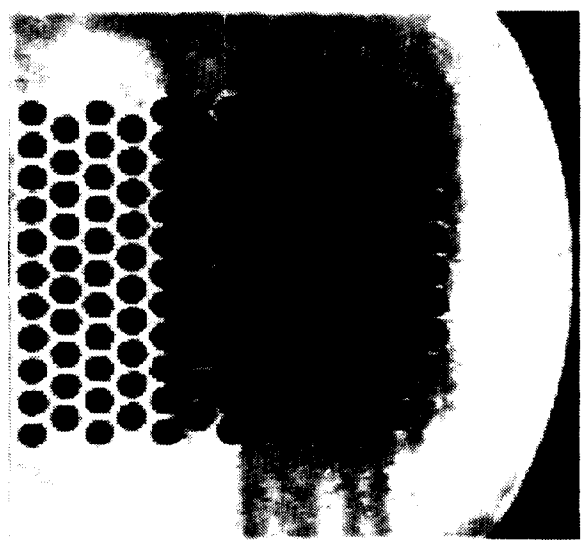

Fig. 7: Defrosting frame of a n accelerator grid showing the left water manifold and the cooling channels.

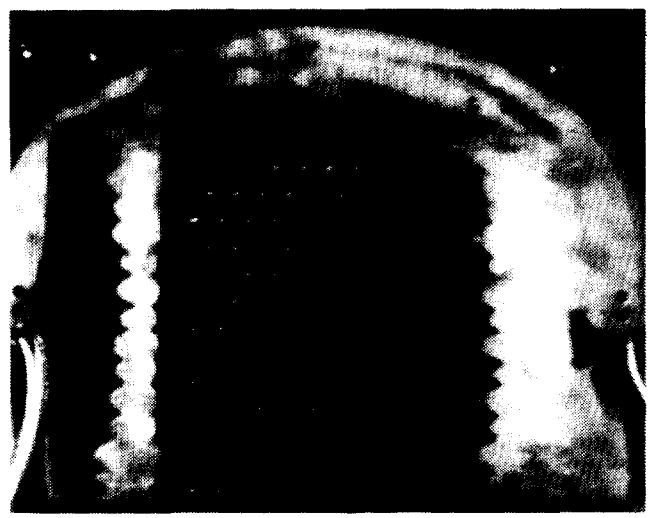

1 A Cardella et al , Fusion Technology 1992, pp 211- 215 Proceedings of the 17th SOFT, Rome, Italy, 14-18 Sept. 1992.

2 M Araki et al, Fusion Technology 1992, pp 166 - 170, Proceedings of the 17th SOFT, Rome, Italy, 14-18 Sept. 1992G.

3 P Adorno et al, Fusion Technology 1992, pp 339 - 343, Proceedings of the 17th SOFT, Rome, Italy, 14-18 Sept. 1992.

4 Panasonic video cassette recorder AG - 7355, COHU 4710 CCIR series monochrome solid state CCD camera.

Temperature profile (top) and the light emission after exposure (bottom) confirm that the thermal contact of tiles 3 and 4 is strongly reduced, that of tiles 6 and 10 is slightly reduced compared to the good tiles.

In all tests we observed that end tiles defrost considerably faster. This is clearly seen in Fig. 2. A consequence of that is, that a fault on the end tiles is somewhat harder to identify.

We can also see in Fig. 3 that the defrosting starts from the point which is closest to the cooling pipe. The first (top) picture of the defrosting sequence shows clearly that the side surface defrosts faster than the top surface. The reason is the reduced distance between surface and cooling pipe which is 6.8 mm for the top surface and 3.2 mm for the side surface. Both observations clearly prove, that the time of defrosting is defined by temperature rather than surface conditions.

Fig. 3: Defrosting sequence of a CFC test section pre-cooled to - 15 °C with the temperature profile after exposure at the top, the defrosting sequence in the middle and the light emission after beam exposure at the bottom.

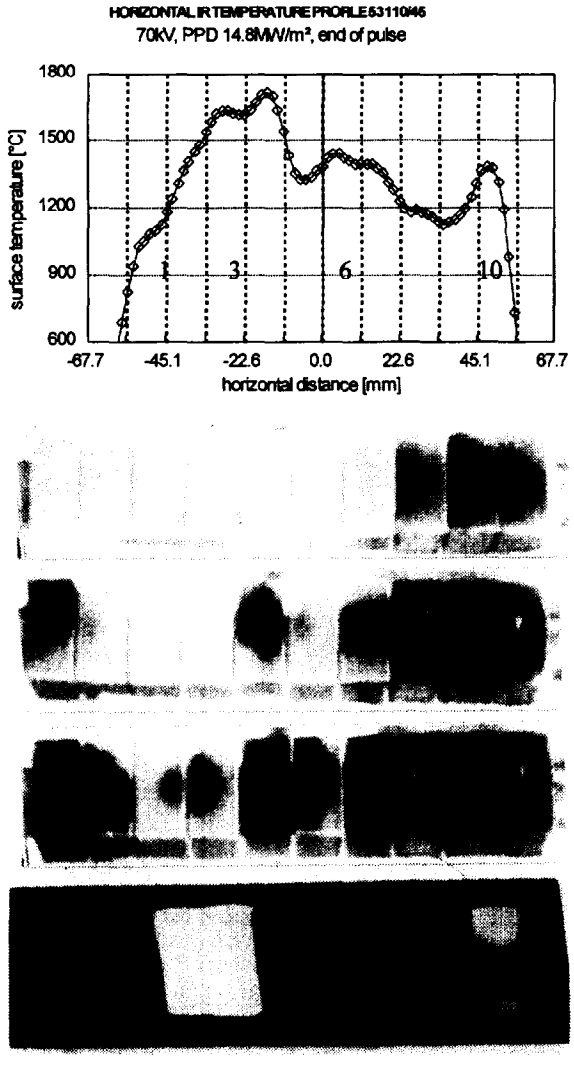

3.2 Accelerator grids

The accelerator grids of the JET beam injection sources are actively cooled. Small cooling channels are embedded into the copper as shown in Fig. 4. The grids are made by electro-deposition with the cooling channels filled with a conducting wax onto the copper base plate. Then copper is built up by electrodeposition over the top of the base plate and the cooling channels. After the electrodeposition the wax is removed. The wax does not give a good contrast on X-ray pictures and it is difficult to check if the wax has been removed quantitatively. To check if the defrosting method could be applied, we deliberately left some water in the cooling channels of the grid prior to cooling the grids. This water will cause some blockage of cooling channels which should be identified by the defrosting test.

Fig. 4: Schematic of the actively cooled JET injector grids showing the cooling channels between the grid holes.

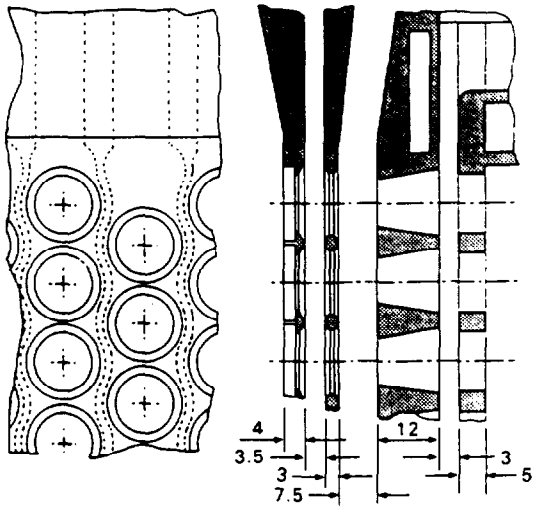

Grid No.	1	2	3	4	
Voltage	80	73	-2	0	kV
Cooling Channel Depth	1.8	1.4	2.4	2.4	mm
Cooling Channel Width	1.4	1.4	2.4	2.4	mm